Enhancing keV high harmonic signals generated by long-wave infrared lasers

ZENGHU CHANG[*]

Institute for the Frontier of Attosecond Science and Technology, CREOL and Department of Physics, University of Central Florida, 4111 Libra Drive, PS430, Orlando, FL 32816, USA
[*]*Zenghu.Chang@ucf.edu*

Abstract: It is indicated by single-atom simulations that the intensity of a single isolated X-ray pulse in the 3.4 to 4 keV region from an 8 micron laser driven high harmonic generation can be increased by more than two orders of magnitude when a single-cycle pulse centered at 800 nm is added. The ionization probability of a helium atom by the two-pulse field is set to 4.56×10^{-5}, which is needed for balancing the index of refraction of free electrons with that of neutral helium atoms to achieve phase matching.

1.   Introduction

Since first demonstrated in 2001, table-top attosecond light sources have relied on high harmonic generation (HHG) in noble gases interacting with near-infrared (NIR) Ti:Sapphire lasers centered at 800 nm [1,2]. The attosecond spectrum with sufficient flux for transient absorption and streaking experiments is limited to the extreme ultraviolet region (XUV) (10 to 150 eV). It was experimentally demonstrated that the cutoff photon energy of high harmonics in the extreme ultraviolet region can be dramatically extended by driving the non-perturbative nonlinear process with long wavelength lasers [3], and the results were explained by using the semi-classical model [4,5]. In the last decade, mJ-level driving lasers centered in the 1.3 to 4 μm range have been developed for generating X-ray pulses in the water-window region (282 to 533 eV) and beyond [6–10]. Long-wave infrared (LWIR) lasers centered at 8 μm are being designed [11] to develop X-ray sources covering the photon energy range of 1 to 5 keV.

It is observed experimentally that the conversion efficiency of the high harmonic generation may decrease when the driving laser wavelength is increased [3], which was attributed to effects of quantum diffusion of electron wave packets. This topic has been studied both theoretically and experimentally [12,13]. As the driving laser wavelength moves from near infrared to mid-wave (3–8 μm) and long-wave (8–15 μm), innovative schemes are needed to achieve useful photon flux. Multi-color laser fields have also been extensively investigated to increase the high harmonic yield and to extend the cutoff [14,15]. The high harmonic generation signal in the plateau region can be enhanced by driving the process with a combination of a strong infrared (IR) and a weak attosecond extreme ultraviolet (XUV) pulse train [16–18] or single isolated sub-femtosecond vacuum ultraviolet (VUV) pulses [19,20]. Since the duration of the XUV/VUV pulse is much shorter than the IR optical period, the particular ionization time can be fixed by properly setting the time delay between the two pulses. The typical intensities of the IR and XUV (or VUV) are 10^{14} W/cm^2 and 10^{13} W/cm^2 respectively. Numerical simulation also shows that a few-cycle 400 nm pulse added to a stronger 2000nm pulse can enhance the high harmonic signal in the 100 to 400 eV region [21]. In addition, it has been demonstrated theoretically that the cutoff of the high harmonic generated by an intense 800 nm pulse can be extended by a 10 times weaker 8 micron pulse to generate isolated XUV attosecond pulses in the 23 to 93 eV range [22]. Here we consider the case where high harmonic generation for producing keV X-rays is driven by a long-wave infrared laser. It is found that the intensity of a single isolated keV X-ray pulse can be

significantly enhanced by adding a single-cycle carrier-envelope phase (CEP) stable NIR laser centered at 800 nm with peak intensities that are a few times less than that of the 8 μm laser.

2. Ionization probability for phase matching of high harmonic generation

High harmonic generation in helium atoms driven by LWIR lasers is studied in this work. The index of refraction of helium gas has been measured at 633 nm [23] and 10.7 micron [24]. However, its value at 8 micron is hard to find in literatures and is estimated by assuming that the frequency dependence of the index of refraction of neutral helium can be approximately expressed by a single-resonance classical electron oscillator equation [25]

$$n_a(\omega_L) = 1 + \frac{e^2}{2\varepsilon_0 m_e} \frac{N_a}{\omega_r^2 - \omega_L{}^2},$$ (1)

where e and m_e are the charge and mass of an electron respectively. ε_0 is the permittivity of free space. N_a is the atomic number density of the unionized atom. ω_L and ω_r are the angular frequency of the laser and the resonant frequency of the atom respectively. The resonant photon energy $\hbar\omega_r = 22.963$ eV is obtained by using the measured index of refraction at 10.7 μm.

The ionization probability, p_{pm}, of the helium atom is fixed when the high harmonic signals generated by a pulse centered at 8 micron alone are compared with that produced by a combination of 8 micron and 800 nm pulses. To achieve phase matching in high harmonic generation [8,26], the value of p_{pm} is chosen so that the index of refraction of the unionized portion of the gas at 8 μm cancels that of the ionized portion, which can be calculated by [25]

$$p_{pm}(\omega_L) = \left(\frac{\hbar\omega_L}{\hbar\omega_r}\right)^2.$$ (2)

It results in $p_m = 4.556 \times 10^{-5}$.

The high harmonic signals generated by a driving laser field centered at 8 μm alone serves as the reference to demonstrate the effects of the additional NIR pulse. The LWIR field and the ionization probability of a helium atom is shown in Fig. 1(a).
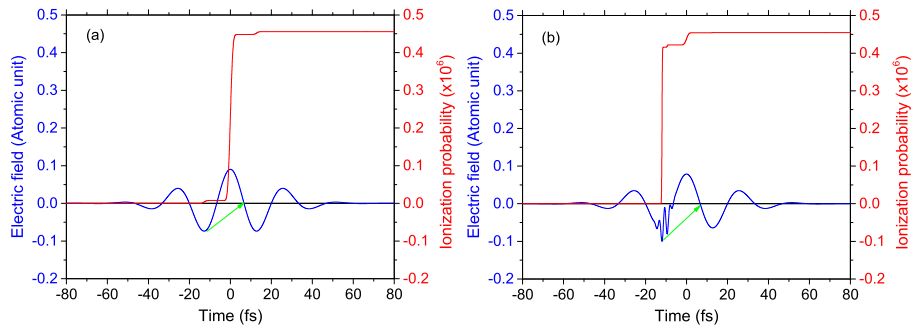

Fig. 1. (a) A 34 fs LWIR driving laser field centered at 8 μm (blue line) and the ionization probability of a helium atom (red line). The peak intensity is 2.86×10^{14} W/cm². The carrier envelope phase is 0 rad. (b) A 3.4 fs NIR pulse centered at 800 nm is added to a LWIR pulse whose intensity is 2.18×10^{14} W/cm². The intensity of the NIR pulse is 1/3 that of the LWIR pulse. The CEP of the NIR pulse is -0.982 rad. The peak of the NIR pulse envelope is 10.67 fs ahead of the LWIR pulse. The green arrows indicate the times of electron release and re-collision for generating a single X-ray pulse.

In few-cycle, near-infrared driven high harmonic generation, a single isolated XUV attosecond pulse is generated when the cutoff region of spectrum is used and the CEP is set proposedly

to form a "cosine wave," which is known as "amplitude gating [27]." The FWHM duration, and carrier envelope phase (CEP) of the LWIR pulse are 34 fs, and 0 rad respectively, such a single-cycle pulse allows generation of isolated attosecond keV X-ray pulses with the amplitude gating and atto-chirp compensation, which is important for pump-probe experiments. When the HHG is driven by the 8 micron pulse only, the peak intensity of the laser is set at 2.86×10^{14} W/cm^2 so that ionization probability at the end of the pulse is 4.56×10^{-5}. The corresponding peak amplitude of the laser field around time zero allows the generation of a keV X-ray burst when an electron is released and recombined as times indicated by the (green) arrow in Fig. 1(a).

When a 3.4 fs NIR pulse centered 800 nm is added to the 8 micron pulse to enhance the HHG signal, the peak intensity of the latter needs to be reduced to maintain the same final ionization probability. The combined electric field is illustrated in Fig. 1 (b). The intensities of the LWIR and NIR pulses are 2.18×10^{14} W/cm^2 and 7.27×10^{13} W/cm^2 respectively. The carrier-envelope phase of the NIR pulse is -0.982 rad. The peak of the NIR pulse envelope is 10.67 fs ahead of the LWIR pulse. The CEP and delay values are chosen to optimize the HHG enhancement as described in section 3. Since the 800 nm pulse duration, 3.4 fs, is shorter than a quarter of optical cycle of the 8 micron light, 5 fs, the tunneling ionization induced by the NIR field is localized that may enhance the emission of a single X-ray burst corresponding to the release and rescattering of an electron at times indicated by the (green) arrow in Fig. 1(b). It is worth mentioning that the added NIR does not change the ionization of the atom during the -1/4 to + 1/4 cycle of the 8 micron field. In other words, the ionization and acceleration steps are decoupled. The former is controlled by the NIR and the latter is determined by the LWIR.

For the generation of single isolated keV X-ray bursts that can potentially be compressed to attosecond pulses by compensating the atto-chirp, the carrier-envelope phase of the driving laser should not change significantly during the propagation in the weekly ionized helium gas target. The calculated CEP change in a 1 mm long cell filled with 5 atm helium gas is 0.27 rad for the 8 micron pulses when the ionization probability is 4.556×10^{-5}, which is typical for a CEP locked laser. The corresponding CEP shift of the 800 nm pulse is 0.04 rad. The group delay difference between the 8 micron and the 800 nm pulses is ~0.02 optical period of the 8 micron light.

3.   Numerical simulations of X-ray signal enhancement

Numerical simulations based on the Strong Field Approximation of high harmonic generation [28] have been performed to demonstrate the enhancement of keV X-ray signals by adding a NIR laser pulse to a LWIR field. The time domain dipole moment of a single helium interacting with a LWIR laser pulse alone or a combined LWIR and NIR field was calculated using the open-source code, HHGmax [29]. The dipole matrix element is hydrogen-like and the ionization potential of the atom is 24.59 eV.

In Fig. 2(a), the power spectrum of the high harmonics generated with the LWIR pulse alone (yellow line) is plotted together with that from the two-pulse driving field (blue line). The sudden change of the spectral intensity at 2.6 keV for the two-pulse case and 3.4 keV for the one-pulse driving case are signatures of the half-cycle cutoffs [30]. Each plateau corresponds to one X-ray burst. The laser parameters are identical to that for Fig. 1. The X-ray intensity in the 3.4 to 4 keV region is increased by more than two orders of magnitude when the 800 nm pulse is added, which is because the probability of releasing an electron at the desired time as indicated by the (green) arrows in Fig. 1 in much larger for the two-pulse driver case. The cutoff photon energy reaches 5.4 keV for the 8 micron laser generated harmonics, which agrees with the semi-classical cutoff law. The cutoff is reduced to 4.1 keV when the high harmonic generation is driven by the two-pulse field because LWIR intensity is reduced. The Fourier transforms of the spectra of the last plateau before the cutoff (3.4 to 5.4 keV for the 8 micron alone and 2.6 to 4.2 keV for the two-color driver) are shown in Fig. 2(b). In addition to the field amplitude increase, the X-ray

pulse duration is shortened by about a factor of two when the 800 nm pulse is added, which is due the suppression of the long quantum trajectory.
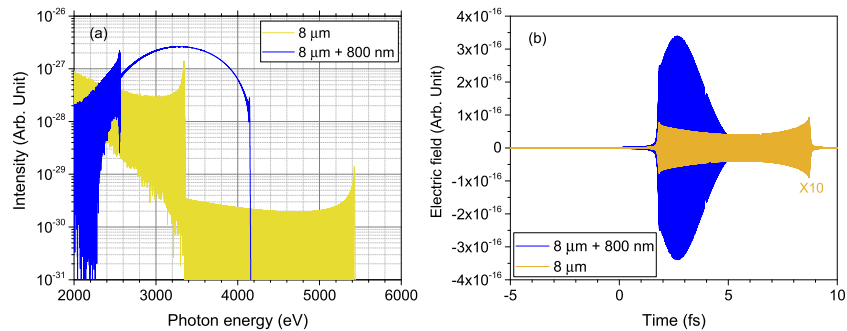

Fig. 2. (a) Power spectra of the high harmonics generated with a LWIR pulse alone (yellow line) and with a LWIR pulse combined with a NIR pulse. The laser parameters are explained in Fig. 1. (b) X-ray pulses corresponding to the spectra in the plateau adjacent to the cutoff.

Both the X-ray spectral shape and intensity depend strongly on the carrier-envelope phase of the 800 nm pulses, as shown in Fig. 3 (a). They are also sensitive to the CEP of the LWIR pulse, and are affected by the time delay between the two pulses. Therefore, the three parameters must be stabilized in experiments. CEP stable few-cycle lasers centered at 800 nm have been the working horse for generating single isolated attosecond pulses [2].
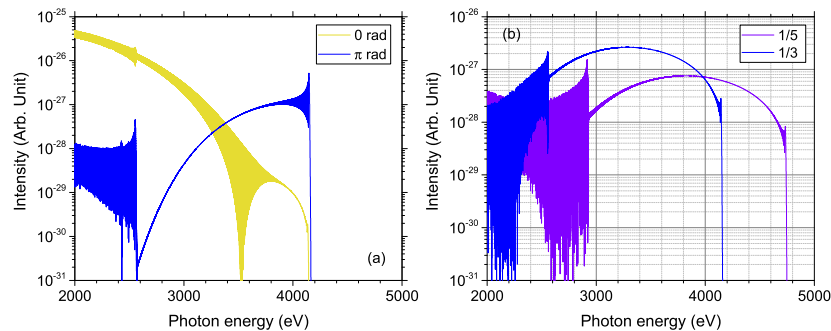

Fig. 3. High harmonic spectra generated with the combined 8 micron and 800 nm pulses. (a) The CEP of the 800 nm pulse is changed. (b) The intensity ratio between the 800 nm and 8 micron pulses is varied.

At a given ionization probability, the intensity of the 800 nm pulse can be chosen by finding an acceptable compromise between the cutoff photon energy and the X-ray signal strength. The comparison of high harmonic spectra generated with the combined fields at two different NIR intensities is shown in Fig. 3(b). When the intensity of the 800 nm pulse is one fifth of the 8 micron pulse, the cutoff reaches a higher value than that when the intensity ratio is one to three, but the enhancement of the X-ray intensity is less (but still more than two orders of magnitude around 4 keV).

The requirement of the intensity of the 34 fs pulses centered at 8 μm∼ 2.2×10^{14}W/cm^2, can be satisfied by focusing a 1 mJ beam to the gas target with an *f/#*=100 optics. It is expected that such pulses could be generated by Optical Parametric Chirped Pulse Amplifiers based on the highly nonlinear material ZnGeP$_2$ [11]. The spectrum of a single-cycle pulse center at 8 μm extends from 4 to 12 μm where the transmission of the crystal ends [11]. The enhancement scheme may be implemented at other wavelengths as long as the difference between the center wavelengths of

the NIR and LWIR is sufficiently large. The less intense quasi-single-cycle 800 nm pulse can be generated with Ti:Sapphire lasers followed by a hollow-core fiber compressor, which seeds the 8 μm laser [11].

It is known from the semi-classical model of high harmonic generation that an electron ionized during the -1/2 to -1/4 cycle (-13 to -7 fs) of the LWIR oscillation experiences the most intense part of the 8 μm laser field around time zero as illustrated in Fig. 1. This is the time range that the NIR should arrive to enhance the X-ray signals. The time delay between the NIR and LWIR pulses, 10.67 fs, is chosen to achieve enhancement of the X-rays peak at 3.3 keV emitted by the short trajectories as shown in Fig. 2. A shorter delay increases the X-ray signals at a lower photon energy. When the seed pulses of the 8 μm laser are generated with the 800 nm laser such as the architecture described in [11], precise synchronization of the two pulses can be accomplished optically.

4.   Summary

The long optical period of the 8 micron laser (26.6 fs) allows the control of ionization within a quarter of a cycle by a 3.4 fs pulse centered at 800 nm to enhance the intensity of a single X-ray burst. With the recent progress on high energy picosecond 2 μm pump lasers, it is expected that Optical Parametric Chirped Pulse Amplifiers centered at 8 μm may soon become available. The single atom simulations in this study are done at the phase matching ionization probability, further investigation will be conducted to study the effects of propagation on the X-ray yield.

Funding

References

1. F. Krausz and M. Ivanov, "Attosecond physics," Rev. Mod. Phys. **81**(1), 163–234 (2009).
2. Z. Chang, P. B. Corkum, and S. R. Leone, "Attosecond optics and technology: progress to date and future prospects [Invited]," J. Opt. Soc. Am. B **33**(6), 1081–1097 (2016).
3. B. Shan and Z. Chang, "Dramatic extension of the high-order harmonic cutoff by using a long-wavelength driving field," Phys. Rev. A **65**(1), 011804 (2001).
4. P. B. Corkum, "Plasma perspective on strong field multiphoton ionization," Phys. Rev. Lett. **71**(13), 1994–1997 (1993).
5. K. Schafer, B. Yang, L. DiMauro, and K. Kulander, "Above threshold ionization beyond the high harmonic cutoff," Phys. Rev. Lett. **70**(11), 1599–1602 (1993).
6. E. J. Takahashi, T. Kanai, K. L. Ishikawa, Y. Nabekawa, and K. Midorikawa, "Coherent water window X ray by phase-matched high-order harmonic generation in neutral media," Phys. Rev. Lett. **101**(25), 253901 (2008).
7. H. Xiong, H. Xu, Y. Fu, J. Yao, B. Zeng, W. Chu, Y. Cheng, Z. Xu, E. J. Takahashi, and K. Midorikawa, "Generation of a coherent x ray in the water window region at 1 kHz repetition rate using a mid-infrared pump source," Opt. Lett. **34**(11), 1747–1749 (2009).
8. T. Popmintchev, M.-C. Chen, A. Bahabad, M. Gerrity, P. Sidorenko, O. Cohen, I. P. Christov, M. M. Murnane, and H. C. Kapteyn, "Phase matching of high harmonic generation in the soft and hard X-ray regions of the spectrum," Proc. Natl. Acad. Sci. **106**(26), 10516–10521 (2009).
9. X. Ren, J. Li, Y. Yin, K. Zhao, A. Chew, Y. Wang, S. Hu, Y. Chen, E. Cunningham, Y. Wu, M. Chini, and Z. Chang, "Attosecond light sources in the water window," J. Opt. **20**(2), 023001 (2018).
10. T. Popmintchev, M.-C. Chen, D. Popmintchev, P. Arpin, S. Brown, S. Ališauskas, G. Andriukaitis, T. Balčiunas, O. D. Mücke, and A. Pugzlys, "Bright coherent ultrahigh harmonics in the keV x-ray regime from mid-infrared femtosecond lasers," Science **336**(6086), 1287–1291 (2012).
11. Y. Yin, A. Chew, X. Ren, J. Li, Y. Wang, Y. Wu, and Z. Chang, "Towards terawatt sub-cycle long-wave infrared pulses via chirped optical parametric amplification and indirect pulse shaping," Sci. Rep. **7**(1), 45794 (2017).
12. J. Tate, T. Auguste, H. Muller, P. Salieres, P. Agostini, and L. DiMauro, "Scaling of wave-packet dynamics in an intense midinfrared field," Phys. Rev. Lett. **98**(1), 013901 (2007).

13. A. Shiner, C. Trallero-Herrero, N. Kajumba, H.-C. Bandulet, D. Comtois, F. Légaré, M. Giguère, J. Kieffer, P. Corkum, and D. Villeneuve, "Wavelength scaling of high harmonic generation efficiency," Phys. Rev. Lett. **103**(7), 073902 (2009).

14. G. Orlando, P. Corso, E. Fiordilino, and F. Persico, "A three-colour scheme to generate isolated attosecond pulses," J. Phys. B: At., Mol. Opt. Phys. **43**(2), 025602 (2010).

15. F. Brizuela, C. Heyl, P. Rudawski, D. Kroon, L. Rading, J. Dahlström, J. Mauritsson, P. Johnsson, C. Arnold, and A. L'Huillier, "Efficient high-order harmonic generation boosted by below-threshold harmonics," Sci. Rep. **3**(1), 1410 (2013).

16. K. J. Schafer, M. B. Gaarde, A. Heinrich, J. Biegert, and U. Keller, "Strong field quantum path control using attosecond pulse trains," Phys. Rev. Lett. **92**(2), 023003 (2004).

17. M. B. Gaarde, K. J. Schafer, A. Heinrich, J. Biegert, and U. Keller, "Large enhancement of macroscopic yield in attosecond pulse train–assisted harmonic generation," Phys. Rev. A **72**(1), 013411 (2005).

18. A. Heinrich, W. Kornelis, M. Anscombe, C. Hauri, P. Schlup, J. Biegert, and U. Keller, "Enhanced VUV-assisted high harmonic generation," J. Phys. B: At., Mol. Opt. Phys. **39**(13), S275–S281 (2006).

19. L. Feng and Y. Li, "High-intensity isolated attosecond X-ray pulse generation by using low-intensity ultraviolet–mid-infrared laser beam," Eur. Phys. J. D **72**(9), 167 (2018).

20. P. Lan, P. Lu, W. Cao, and X. Wang, "Efficient generation of an isolated single-cycle attosecond pulse," Phys. Rev. A **76**(4), 043808 (2007).

21. H. Du, L. Luo, X. Wang, and B. Hu, "Attosecond ionization control for broadband supercontinuum generation using a weak 400-nm few-cycle controlling pulse," Opt. Express **20**(24), 27226–27241 (2012).

22. E. Balogh, K. Kovacs, P. Dombi, J. A. Fulop, G. Farkas, J. Hebling, V. Tosa, and K. Varju, "Single attosecond pulse from terahertz-assisted high-order harmonic generation," Phys. Rev. A **84**(2), 023806 (2011).

23. K. P. Birch, "Precise determination of refractometric parameters for atmospheric gases," J. Opt. Soc. Am. A **8**(4), 647–651 (1991).

24. S. Marchetti and R. Simili, "Accurate measurement of the refractive index of CO_2, N_2, He, O_2, and air at 10.57 μ and T = 23° C," Infrared Phys. Technol. **47**(3), 263–266 (2006).

25. Z. Chang, *Fundamentals of Attosecond Optics* (CRC Press, 2011).

26. A. Rundquist, C. G. Durfee, Z. H. Chang, C. Herne, S. Backus, M. M. Murnane, and H. C. Kapteyn, "Phase-matched generation of coherent soft X-rays," Science **280**(5368), 1412–1415 (1998).

27. M. Chini, K. Zhao, and Z. Chang, "The generation, characterization and applications of broadband isolated attosecond pulses," Nat. Photonics **8**(3), 178–186 (2014).

28. M. Lewenstein, P. Balcou, M. Y. Ivanov, A. L'huillier, and P. B. Corkum, "Theory of high-harmonic generation by low-frequency laser fields," Phys. Rev. A **49**(3), 2117–2132 (1994).

29. M. Hoegner, https://github.com/Leberwurscht/HHGmax. https://www.attoworld.de/fileadmin/user_upload/tx_attoworld/publications/thesis_master_en_Y2013_LMU_FakPhys_HoegnerMaximilian.pdf.

30. C. Haworth, L. Chipperfield, J. Robinson, P. Knight, J. Marangos, and J. Tisch, "Half-cycle cutoffs in harmonic spectra and robust carrier-envelope phase retrieval," Nat. Phys. **3**(1), 52–57 (2007).